

Review

# Recent Progress in Lanthanide-Doped Inorganic Perovskite Nanocrystals and Nanoheterostructures: A Future Vision of Bioimaging

Gowri Manohari Arumugam <sup>1</sup>, Santhosh Kumar Karunakaran <sup>2</sup>, Raquel E. Galian <sup>1,\*</sup>  
and Julia Pérez-Prieto <sup>1,\*</sup>

<sup>1</sup> Instituto de Ciencia Molecular (ICMol), University of Valencia, Catedrático José Beltrán, 2, Paterna, 46980 Valencia, Spain; gowrimanohari1987@gmail.com

<sup>2</sup> State Key Laboratory of Optoelectronic Materials and Technologies, Nanotechnology Research Center, School of Materials Science & Engineering, Sun Yat-sen University, Guangzhou 510275, China; sanstechno@gmail.com

\* Correspondence: raquel.galian@uv.es (R.E.G.); julia.perez@uv.es (J.P.-P.)

**Abstract:** All-inorganic lead halide perovskite nanocrystals have great potential in optoelectronics and photovoltaics. However, their biological applications have not been explored much owing to their poor stability and shallow penetration depth of ultraviolet (UV) excitation light into tissues. Interestingly, the combination of all-inorganic halide perovskite nanocrystals (IHP NCs) with nanoparticles consisting of lanthanide-doped matrix (Ln NPs, such as NaYF<sub>4</sub>:Yb,Er NPs) is stable, near-infrared (NIR) excitable and emission tuneable (up-shifting emission), all of them desirable properties for biological applications. In addition, luminescence in inorganic perovskite nanomaterials has recently been sensitized via lanthanide doping. In this review, we discuss the progress of various Ln-doped all-inorganic halide perovskites (LnIHP). The unique properties of nanoheterostructures based on the interaction between IHP NCs and Ln NPs as well as those of LnIHP NCs are also detailed. Moreover, a systematic discussion of basic principles and mechanisms as well as of the recent advancements in bio-imaging based on these materials are presented. Finally, the challenges and future perspectives of bio-imaging based on NIR-triggered sensitized luminescence of IHP NCs are discussed.

**Keywords:** inorganic perovskite; lanthanide-doped nanocrystals; upconversion photoluminescence; nanoheterostructure



**Citation:** Arumugam, G.M.; Karunakaran, S.K.; Galian, R.E.; Pérez-Prieto, J. Recent Progress in Lanthanide-Doped Inorganic Perovskite Nanocrystals and Nanoheterostructures: A Future Vision of Bioimaging. *Nanomaterials* **2022**, *12*, 2130. <https://doi.org/10.3390/nano12132130>

Academic Editor: Mohammed Jaouad Meziani

Received: 18 May 2022

Accepted: 15 June 2022

Published: 21 June 2022

**Publisher's Note:** MDPI stays neutral with regard to jurisdictional claims in published maps and institutional affiliations.



**Copyright:** © 2022 by the authors. Licensee MDPI, Basel, Switzerland. This article is an open access article distributed under the terms and conditions of the Creative Commons Attribution (CC BY) license (<https://creativecommons.org/licenses/by/4.0/>).

## 1. Introduction

Nowadays, IHP NCs are considered prospective materials not only for photovoltaic applications but also for nanophotonics and nonlinear optics. Moreover, these nanomaterials have steadily attracted the research communities because of their unique physical properties such as high photoluminescence quantum yield (PLQY), tuneable PL and defect tolerance [1,2]. In particular, lead halide perovskite NCs are especially attractive for high-performance solar cells, lasers, photodetectors and light-emitting diodes (LEDs) owing to their superior optical properties including high PLQY, large absorption cross-section and tuneable emission throughout the entire visible spectrum [3–7], though these perovskites have poor stability, which limit their general application. IHP NCs usually exhibit linear optical properties under UV and visible light. It is important to note that near-infrared (NIR) photon upconversion is a unique process that converts two or more NIR photons into one of a higher energy, thus leading to anti-Stokes emissions. It is very difficult to achieve nonlinear upconversion (UC) emissions in IHP materials because of their low multiphoton efficiency and lack of intermediate energy levels [8–11].

Nanoparticles comprising an inorganic matrix such as NaYF<sub>4</sub> and NaYbF<sub>4</sub> with two or more lanthanide ions as dopants such as Yb/Tm, Yb/Er, etc., present higher stability than

that of IHP NCs as well as higher multiphoton absorption efficiency [12]. The NIR-excitation of Ln NPs using a continuous-wave laser as an excitation source yielded UC emissions in the NIR-to-UV range. Ln NPs have generally been used in biological applications such as bio-imaging and phototherapy owing to the considerable penetration depth of NIR light into biological systems [13–16]. However, the fluorescence emissions of Ln NPs have fixed wavelengths as well as non-tuneable emission colours due to limited energy levels of lanthanide ions, which restricted their usage in multiplexed bioimaging or bioassays [17,18]. The wavelength tuning of Ln NP emissions requires select Ln ions and suitable doping concentrations.

Although the optoelectronic applications of IHP NCs have been well explored, their bio-applications are limited by the lead toxicity and their low stability under humidity, light and heat. Clearly, the major drawback of the perovskites is their poor stability, which accumulates decomposition. Perovskites can cause toxicity in biological applications since they degrade when exposed to water due to their ionic nature [19–21]. However, the superior optical properties of IHP NCs provide several advantages to be used in the field of bioimaging. Nevertheless, there are many issues, such as the stability of these materials under physiological conditions, their integration in biomolecules during circulation, their epigenetic interaction and their possible toxicity during degradation processes, to be clarified before real life implementation [22]. Interestingly, the combination of perovskites and Ln NPs can solve the abovementioned issues through the formation of nanoheterostructures with superior optical properties. Tuning the UC emission wavelengths under NIR light excitation is a promising strategy [23–25]. In addition, the combination of IHP NCs and Ln NPs achieved UC emissions, and it can also endow perovskite NCs with long-term stability [26].

The aim of this work is to review the unique properties of nanoheterostructures based on the interactions between IHP NCs and Ln NPs as well as of those of LnIHP NCs. Here, we present a systematic discussion on basic principles and mechanisms as well as on the recent advancements in bioimaging based on these materials and the challenges for facing future developments in bioimaging.

## 2. Metal Halide Perovskite Nanocrystals

Perovskite materials generally have a chemical formula of  $ABC_3$ , in which A and B represent the cations of dissimilar sizes and C denotes the anions such as oxygen and halogens. The ideal perovskite structure is cubic symmetrical, which consists of corner sharing  $BC_6$  octahedra as a backbone with cuboctahedral voids occupied by A-cations, as depicted in Figure 1 [27]. If the A-ion is small or the B-ion is large, the tolerance factor decreases to  $<1$ , which favours orthorhombic, rhombohedral or tetragonal structures rather than a cubic structure.

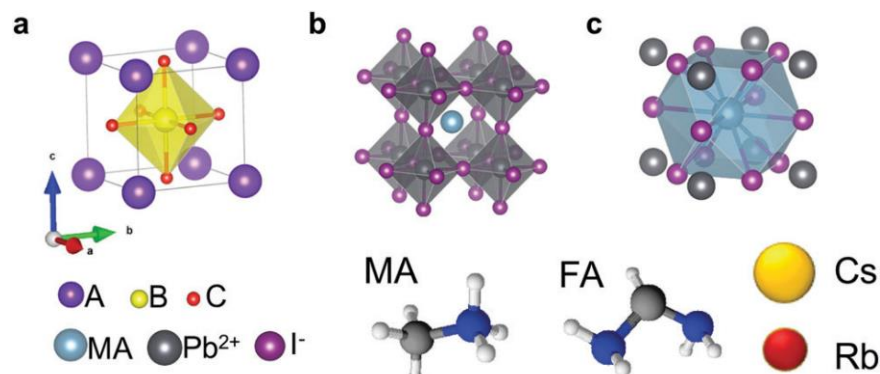


**Figure 1.** Structural features for metal halide perovskites. (a) Unit cell of general cubic perovskite; (b) MAPbI<sub>3</sub> with octahedral coordination around lead ions; (c) MAPbI<sub>3</sub> with cuboctahedra coordination around organic ions. Reprinted with permission [27]. Copyright 2017, Royal Society of Chemistry.

Hybrid perovskites, such as methylammonium/formamidium lead halides (MA/FAPbX<sub>3</sub>) have attracted the interest of researchers because of their excellent performance in optoelectronic devices. This is based on their superior properties: tuneable bandgap, high light absorption capability, long carrier diffusion length and inexpensive raw materials for their preparation. However, they have been affected by instability issues not only in solar cells but also in other applications, such as in LEDs and bioimaging. Inorganic perovskites have been introduced into optoelectronic devices to overcome these issues [28–30]. Inorganic perovskite oxide, lead-free inorganic perovskites and inorganic perovskites with mixed halides have also been developed in past decades [31–38]. All-inorganic halide perovskites have also received great attention from various fields such as solar cells [39,40], lasers [41,42], LEDs [43,44], water splitting [45,46], etc. because of their high performance and stability.

### 2.1. All-Inorganic Halide Perovskites (IHP)

According to the literature, oxide-based perovskites are the most actively studied materials in the perovskite family due to their excellent magnetic, ferro-electric and superconductive properties [47]. Interestingly, the first halide-based perovskite structures were obtained by Moller in caesium lead halides (CsPbX<sub>3</sub>) [48]. The photoconductive properties of halide-based perovskites are tuneable by varying the halide components, which helps to achieve different spectral responses. They have interesting optical properties, including tuneable emission, defect tolerance, quantum confinement effect and high PL quantum efficiency. Remarkably, the emission of CsPbX<sub>3</sub> (X = Cl, Br, I or their mixture) NCs can be tuned from 400 nm to 700 nm, as shown in Figure 2 [1,49].

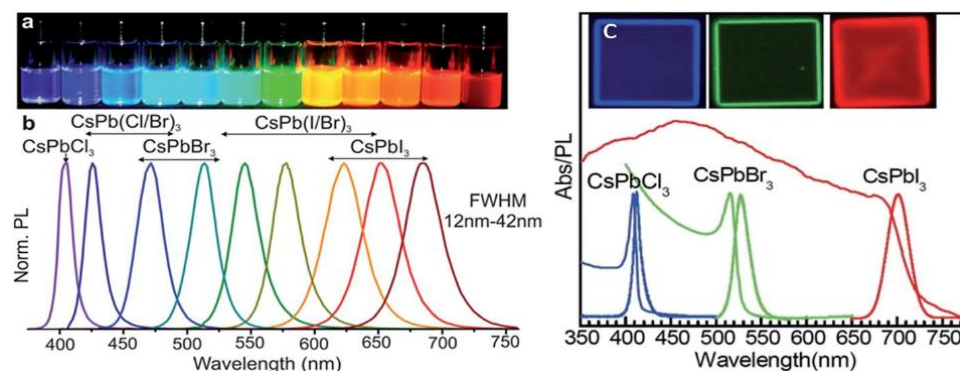


**Figure 2.** (a) Colloidal CsPbX<sub>3</sub> NCs (X = Cl, Br and I) in toluene under UV lamp ( $\lambda = 365$  nm); (b) corresponding PL spectra ( $\lambda_{\text{exc}} = 400$  nm for all but 350 nm for CsPbCl<sub>3</sub> NCs); (c) optical absorption, PL spectra and inset images for CsPbCl<sub>3</sub>, CsPbBr<sub>3</sub> and CsPbI<sub>3</sub> nanoplatelets. Reprinted with permission [49,50]. Copyright 2016, John Wiley & Sons and 2015, American Chemical society.

### 2.2. Ln-Doped Inorganic Halide Perovskites (LnIHPs)

Lanthanide ions have unique properties that come from their 4f electrons and make them an attractive tool for optical applications owing to their large quantum numbers ( $n = 4$ ,  $l = 3$ ) with rich spectroscopic properties [51]. Interestingly, they have advantageous optical properties such as sharp band emissions, large Stokes/anti-Stokes shifts, high luminescent lifetimes and excellent photostability [52,53]. These properties are desirable for their applications in lighting and displays [54], bioimaging [55], therapy [56] and sensing [57]. Furthermore, Ln-doped NPs can serve as multifunctional platforms for bio-applications either by doping or surface functionalization. Ln doping in hybrid perovskites also plays a key role in their optoelectronic properties. For example, MAPbI<sub>3</sub> with lanthanides has been considered a desirable candidate for improving the permanence of perovskite solar cells. The incorporation of various lanthanide ions (Ln<sup>3+</sup> = Ce<sup>3+</sup>, Eu<sup>3+</sup>, Nd<sup>3+</sup>, Sm<sup>3+</sup> or Yb<sup>3+</sup>) into perovskite films largely enhances their performance, such as the efficiency and stability of the device, which is attributed to an enlarged grain size and crystallinity [20].

Interestingly, the inorganic perovskite NCs of  $\text{CsPbX}_3$  ( $X = \text{Cl, Br and I}$ ) exhibited efficient and narrow 4f–4f emissions through sensitization by lanthanide ions, which achieved tremendous success in optoelectronics. Apart from normal Stokes spectral shifting behaviour, the  $\text{CsPbCl}_3$  NCs with  $\text{Yb}^{3+}$  as a dopant exhibited excellent NIR PL with QY of 200% due to quantum cutting phenomena. Beyond that, the IHP also possessed UC photoluminescence with the presence of desirable Ln ions and this review article is mainly focused on UC phenomenon. The crystal lattice of inorganic lead halide perovskites is suitable for lanthanide ion doping due to their octahedral coordination ( $\text{CN} = 6$ ). In particular,  $\text{CsPbX}_3$  NCs showed strong absorption of visible light and intense emission, which can be attributed to their excitonic transitions along with their desirable charge transportation, and hence, they are considered ideal hosts for lanthanide ion doping [58].

Reinhard et al. [59] synthesized  $\text{Yb}^{3+}$ -doped  $\text{Rb}_2\text{MnCl}_4$  perovskite crystals to yield up-conversion luminescence (UCL) under NIR excitation. The crystals exhibited very intense yellow-orange UCL when excited at 15 K. The UC process comprises a sequence of ground state and excited-state absorptions under an excitation with 10 ns pulses. The UC mechanism is cooperative, and both  $\text{Yb}^{3+}$  and  $\text{Mn}^{2+}$  ions in the crystals can participate in the process. The UC in  $\text{Rb}_2\text{MnCl}_4:\text{Yb}^{3+}$  with a linear arrangement of  $\text{Yb}^{3+}\text{-Cl}^-\text{-Mn}^{2+}$  proved to be three orders of magnitude, which is more efficient than that of the  $\text{Yb}^{3+}\text{-(Br}^-\text{)}_3\text{-Mn}^{2+}$  arrangement of face-sharing octahedra in  $\text{CsMnBr}_3:\text{Yb}^{3+}$ . However, three loss processes were observed at temperatures above 50 K: one was intrinsic for  $\text{Rb}_2\text{MnCl}_4$ , whereas the others were related to the presence of  $\text{Yb}^{3+}$  (thermal quenching and non-radiative relaxation). All of these loss processes are governed by basic physical laws and prevent materials containing  $\text{Yb}^{3+}$  and  $\text{Mn}^{2+}$  from being used as an upconverter at room temperature.

Later on, Beurer et al. [60] prepared  $\text{Tm}^{2+}$ -doped  $\text{CsCaI}_3$  and  $\text{RbCaI}_3$  single crystals and compared their properties, such as absorption, light emission and UCL. Both compounds possessed multiple emissions under an excitation at  $21,834\text{ cm}^{-1}$  in the 10 to 300 K temperature range but differed in the dominant UC processes. It can be demonstrated that a slight chemical variation between  $\text{CsCaI}_3:\text{Tm}^{2+}$  and  $\text{RbCaI}_3:\text{Tm}^{2+}$  caused drastic effects on their emissive properties. A relatively modest distortion of  $\text{TmI}_6$  octahedron in  $\text{RbCaI}_3:\text{Tm}^{2+}$  suggests that a reduction in relevant energy gaps between excited states generally influences the competition between radiative and nonradiative relaxation processes.

The combination of  $\text{CsCaI}_3:\text{Tm}^{2+}$  with a low multi-phonon rate constant and  $\text{RbCaI}_3:\text{Tm}^{2+}$  with an efficient UC process can possibly yield an efficient UC phosphor. On the one hand, it requires a smaller distortion of coordination octahedron than in  $\text{RbCaI}_3:\text{Tm}^{2+}$  to prevent a reduction in energy gap. On the other hand, the barycentre of  $(4f)^{12}(5d)^1$  states at low energies in  $\text{RbCaI}_3:\text{Tm}^{2+}$  can enable efficient nonradiative relaxation at the  ${}^2\text{F}_{5/2}$  crystal-field levels. The mixed crystals of  $\text{Tm}^{2+}$ -doped  $\text{RbCaI}_3$  and  $\text{CsCaI}_3$  can tune the energy gaps to optimal values.

Understanding the impact of dopant ions in host materials on energy transitions via the UC process is crucial for further extending the properties and applications of UC materials. In this regard, Gong et al. [61] reported the Er-doped  $\text{PbTiO}_3$  (PTO) perovskite nanofibers as model systems for exploring the effects of tetragonality and polarization on their UCL properties. A clear emission enhancement was observed in the UC green band at 523 nm and in the red band at 656 nm of Er-doped PTO perovskite nanofibers when compared with those in Er-doped  $\text{BaTiO}_3$  or PTO particles. This enhancement is mainly attributed to UC processes assisted by low-energy phonons. These results pave a way for further understanding the energy transition processes between lanthanide dopants and host perovskite oxide matrices in UC processes and for extending the applications of UC materials.

A single-band pure UC emission is beneficial for enhancing colour purity and bioimaging. Interestingly, Wu et al. [62] reported a successful achievement of single-band red UC emission in 2016 from  $\text{Yb}^{3+}/\text{Er}^{3+}$  co-doped  $\text{KMgF}_3$  perovskite NCs. These NCs were prepared by means of a non-equivalent substitution strategy, in which  $\text{Ln}^{3+}$  ions could

aggregate as supported by density functional theory (DFT) calculations and UC dynamic processes. The single-band emission under a laser excitation at 976 nm proved to be independent of dopant concentration and pump power, as shown in Figure 3. The aggregation of  $\text{Ln}^{3+}$  ions and the strong cross-relaxation between them in the  $\text{KMgF}_3$  matrix played important roles for the occurrence of a single-band red emission.

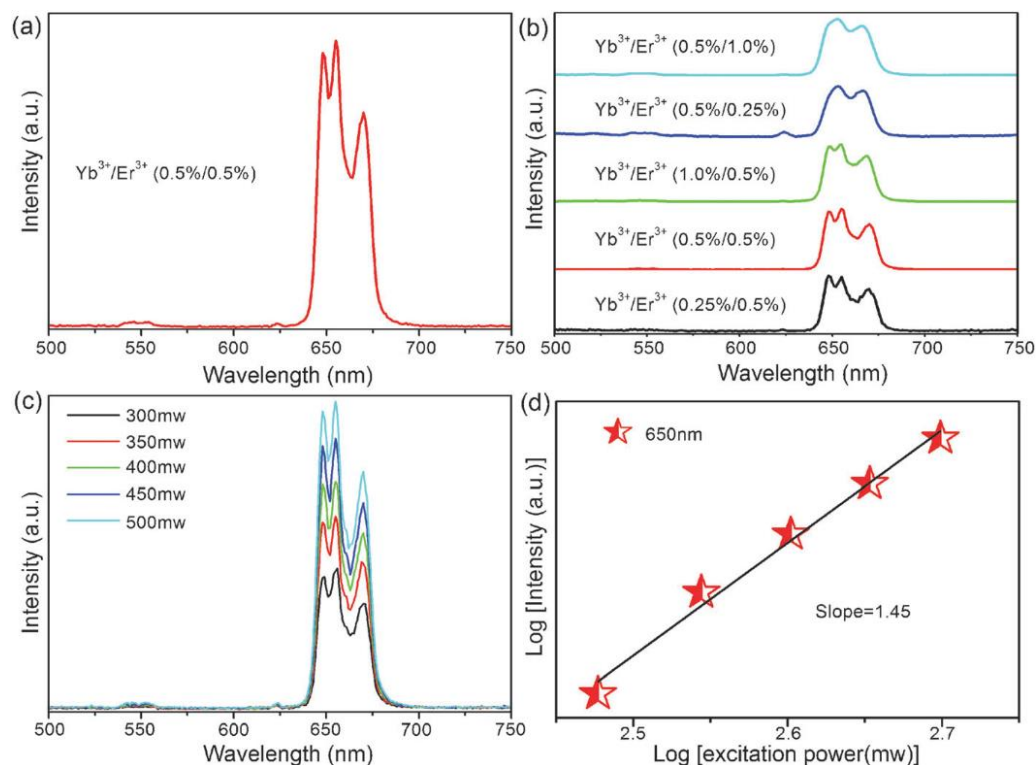


**Figure 3.** UC properties of  $\text{KMgF}_3:\text{Yb}^{3+}, \text{Er}^{3+}$  UCNCs. (a) A spectrum of single-band red UC emission; (b) UC emission spectra with various doping concentrations; (c) UC emission spectra with various excitation powers; (d) the corresponding logarithmic plot between UC intensity and excitation power. Reprinted with permission [62]. Copyright 2016, Royal Society of Chemistry.

Concomitantly, Ge et al. [63] synthesized the Er-doped perovskite single-crystals of  $\text{NaNbO}_3$  nanorods using a hydrothermal method with different doping concentrations. They demonstrated the successful incorporation of  $\text{Er}^{3+}$  ions into the B site of  $\text{Nb}^{5+}$  in the  $\text{ABO}_3$  perovskite structure and then into the A site of  $\text{Na}^+$  by increasing the Er doping concentration. High-resolution transmission electron microscopy (HRTEM) confirmed the single-crystal features of  $\text{NaNbO}_3$  nanorods. These nanorods doped with 0.5 wt% of  $\text{Er}^{3+}$  exhibited a strong green emission and weak red emission, and the studies on the dependence of emission with a laser power corroborated the contribution of two photons. Based on their luminescent properties, these nanorods can be applied in novel multifunctional devices as well as in bioimaging.

Although UC nanostructures play a vital role in bioimaging applications, the enhancement of the red/green UC emission ratio is still challenging. In 2018, Arumugam et al. [64] prepared  $\text{RbPbI}_3:\text{Er}^{3+}, \text{Yb}^{3+}$  nanowires and combined them with surface plasmons to improve the red UC emission at 652 nm which was slightly higher than that of green emission at 548 nm (R/G ratio of 1.068). The UC emission and the mechanism shown in the partial energy level diagram of  $\text{Er}^{3+}$  and  $\text{Yb}^{3+}$  are illustrated in Figure 4. Excitation at 980 nm promotes  $\text{Yb}^{3+}$  ions to the  $^2\text{F}_{5/2}$  level which resonantly conveys its energy to nearby  $\text{Er}^{3+}$  ions through energy transfer up-conversion (ETU) process and fosters them from ground state to  $^4\text{I}_{11/2}$  state. Most of the populations relax down to the level of  $^4\text{I}_{13/2}$  via non-radiative relaxation process. The populations at  $^4\text{I}_{11/2}$  and  $^4\text{I}_{13/2}$  levels absorb a second incident photon to reach  $^4\text{F}_{7/2}$  and  $^4\text{F}_{9/2}$  levels via excited state absorption (ESA) process. Hence,

the populations from  $^2H_{11/2}/^4S_{3/2}$  and  $^4F_{9/2}$  levels relax down to the ground state of  $^4I_{15/2}$  radiatively, resulting in bright red emission with weak-to-moderate green emissions.

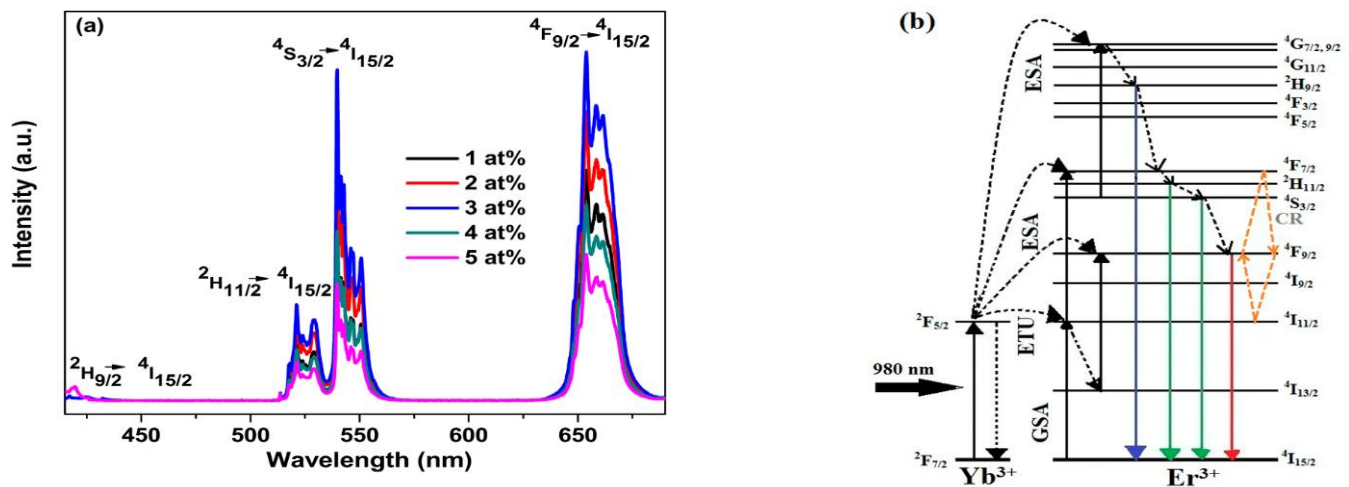


**Figure 4.** (a) UC emission of  $RbPbI_3:Er^{3+}$  (10 at%),  $Yb^{3+}$  with different doping concentrations of ytterbium under an excitation at 980 nm; (b) transition mechanism of UC process ( $RbPbI_3:Er^{3+}, Yb^{3+}$ ) at 980 nm excitation. Reprinted with permission [64]. Copyright 2018, American Institute of Physics.

The red emission was about eight times greater when introducing an oleate complex (to become a surface ligand) in the formation of the  $RbPbI_3:Er^{3+}, Yb^{3+}$  nanowires (NWs). In addition, the decoration of a UC system with AuNPs as surface plasmons greatly improved the red emission, reaching a R/G ratio of 26:1. The reduced green emission lifetime of NWs was consistent with resonance energy transfer from NWs to surface plasmons of Au NPs. By contrast, the addition of surface plasmons accumulated a longer lifetime of the red band emission. The red UC emission enhancement was caused by the addition of surface plasmons, which was assisted by a surface plasmon resonance (SPR) band at 660 nm. Therefore,  $RbPbI_3:Er^{3+}, Yb^{3+}/Au$  NPs are suitable candidates for bioimaging due to their desirable lifetime and enhanced red UC emission.

### 3. Lanthanide-Doped Matrices ( $NaLnF_4$ Matrices, Ln NPs)

UC is an interesting phenomenon of bioimaging as it is a more efficient process than that of two-photon absorption and high harmonic generation. In past decades, numerous bio-probes have been reported, such as fluorescent proteins, dyes and quantum dots, although they are not suitable for life science applications.

UC nanostructures are considered promising materials for bioprobes [65], and in particular,  $Er^{3+}/Yb^{3+}$  co-doped  $NaYF_4$  has been recognized as an efficient UC system although it presents some undesirable background radiation because of its prominent green emission with a lower signal–noise ratio. These drawbacks have encouraged investigations into other UC perovskite matrices. Compared with perovskite oxide materials, the inorganic halide perovskites are suitable for bioimaging because of their excellent photo-stability and higher chemical durability [59]. Host lattices with heavier halides are beneficial for the stabilization of dopant ions [60]. Inorganic halide perovskites are considered promising UC materials for bioimaging because of their adjustable crystal structure, optical stability, resistance to photo-bleaching and photo-blinking, spectral distinguishability and chemical durability [66].

Nanoparticles consisting of lanthanide-doped matrices such as  $NaYF_4:Yb,Er$  NPs have attracted the interest of research communities due to their advantageous properties such as narrow band gap emission, reasonable optical stability and high chemical stability when compared with traditional luminescent materials, e.g., organic dyes and NCs. Moreover, Ln NPs have been widely used in the field of biology owing to their deep penetration into biological tissues without any damage and high signal-to-noise ratio under NIR excitation.

Doping of matrices with lanthanides is the most attractive tool for their optical applications because of large quantum numbers ( $n = 4, l = 3$ ) of lanthanide ions and rich spectroscopic properties [51]. Lanthanides are mostly stable in the +3 oxidation state except for  $\text{Ce}^{4+}$ ,  $\text{Tb}^{4+}$  and  $\text{Yb}^{2+}$  ions. In addition, the size and morphology of Ln NPs play key roles in biomedical applications [67,68].

In early NIR-to-visible UCL bioimaging investigations, it was difficult to achieve tissue penetration depths in the scale of millimetres. However, Yin et al., reported UCL imaging for the first time with considerable tissue depth (a penetration depth of 1 cm) using a luminescent probe of  $\text{NaYF}_4:\text{Yb,Er}$  NPs in nude mice [69]. Concomitantly, Jing et al., compared the UCL imaging of pork muscle tissues at different depths (0–1 cm) through injections of polymer-modified  $\text{NaYF}_4:\text{Yb,Er}$  and  $\text{KMnF}_3:\text{Yb,Er}$ . For the former, the image was detected at a depth of about 0.5 cm, whereas  $\text{KMnF}_3:\text{Yb,Er}$  exhibited a very strong red emission, which was detected at a tissue depth of 1 cm [70]. Xiang et al., have reported the importance of antigen-loaded Ln NPs in labelling and stimulating dendritic cells (DCs), and the Ln NP-labelled DCs achieved high-sensitivity *in vivo* UCL imaging [71].

Subsequently, Hesse et al. [72] reported the rapid preparation of sub-10 nm level pure hexagonal ( $\beta$ -phase)  $\text{NaYF}_4$ -based Ln NPs using a simple one-pot method, in which thermanol 66 was used as a co-solvent and monodispersed Ln NPs were obtained in very short reaction times. The UCL properties of these NPs were tuned by varying the dopant concentrations ( $\text{Nd}^{3+}$  and  $\text{Yb}^{3+}$  as sensitizers, and  $\text{Er}^{3+}$  as an activator). The enhancement in UCL intensity was observed in Ln NPs with optimized concentrations of sensitizer and activator ions as well as coating with inert/active shell. The UCL spectrum of core  $\beta\text{-NaYF}_4:\text{Yb}^{3+}/\text{Er}^{3+}$  20/2% Ln NPs in cyclohexane exhibited three intense bands centred at  $\lambda = 525$  ( $^2\text{H}_{11/2} \rightarrow ^4\text{I}_{15/2}$  transition, G1), 545 ( $^4\text{S}_{3/2} \rightarrow ^4\text{I}_{15/2}$  transition, G2) and 660 nm ( $^4\text{F}_{9/2} \rightarrow ^4\text{I}_{15/2}$  transition, R) under an excitation of 976 nm.

The excitation of conventional Ln NPs such as  $\text{NaYF}_4:\text{Yb}^{3+}/\text{Er}^{3+}(\text{Tm}^{3+})$  at 980 nm caused overheating and damage of living tissues with a reduction in luminescence due to water absorption at 980 nm. Interestingly, the incorporation of  $\text{Nd}^{3+}$  ions into Ln NPs shifted the excitation wavelength to 808 nm, thus minimizing the absorption of water. Hence, Kostiv et al. [73] designed the  $\text{NaYF}_4:\text{Yb}^{3+}/\text{Er}^{3+}@\text{NaYF}_4:\text{Nd}^{3+}$  core-shell NPs doped with  $\text{Yb}^{3+}$  and  $\text{Nd}^{3+}$  as sensitizers, and  $\text{Er}^{3+}$  as an activator for bioimaging. The core was uniform, with a thickness of 24 nm, whereas the core-shell particles had tuneable shell thicknesses of  $\sim 0.5$ –4 nm. They were coated with in-house synthesized poly ethyleneglycol (PEG)-neridronate terminated with alkyne (Alk) to ensure their dispersibility in biological media. The stability of  $\text{NaYF}_4:\text{Yb}^{3+}/\text{Er}^{3+}@\text{NaYF}_4:\text{Nd}^{3+}$ -PEG-Alk NPs in water or 0.01 M PBS, and the presence of PEG on the surface were determined. These Ln NPs were considered non-invasive probes for specific bioimaging of cells and tissues.

#### 4. Nanoheterostructures Based on IHP NCs and Ln NPs

In recent years, all-inorganic  $\text{CsPbX}_3$  ( $X = \text{Cl, Br}$  and  $\text{I}$ ) perovskite NCs have proven to be promising materials in the field of optoelectronics due to their outstanding linear optical properties, even though the nonlinear properties of these perovskites are limited due to their small multiphoton absorption cross section and requirement of high-power density excitation. Interestingly, Zheng et al. [74] proposed a convenient strategy for tuning the UCL in  $\text{CsPbX}_3$  perovskite NCs through the sensitization of  $\text{Ln}^{3+}$ -doped NPs. Particularly,  $\text{CsPbX}_3$  NCs and  $\text{LiYbF}_4:0.5\%\text{Tm}^{3+}@\text{LiYF}_4$  core/shell Ln NPs were dispersed in cyclohexane to lead a homogeneous colloid. The  $\text{CsPbX}_3$ -concentration-dependent UCL spectra for  $\text{LiYbF}_4:0.5\%\text{Tm}^{3+}@\text{LiYF}_4$  core/shell NP- $\text{CsPbBr}_3$  perovskite NCs were obtained under excitation at 980 nm, as depicted in Figure 5. Full-colour emissions with wavelengths beyond the availability of lanthanide ions were attained by adjusting the band gap of IHP NCs. These results presented the first panorama for photon UC with high efficiency, multiple colours and a tuneable lifetime of perovskite NCs under an excitation at low power density. It is important to note that the IHP NC luminescent lifetime was lengthened from the intrinsic nanosecond scale to milliseconds due to radiative energy transfer (RET)

from Ln-doped NPs to IHP NC. This work opens a new avenue for the exploration of perovskite NCs based on UCL toward versatile applications such as ultrasensitive bioassay and high-resolution bioimaging.

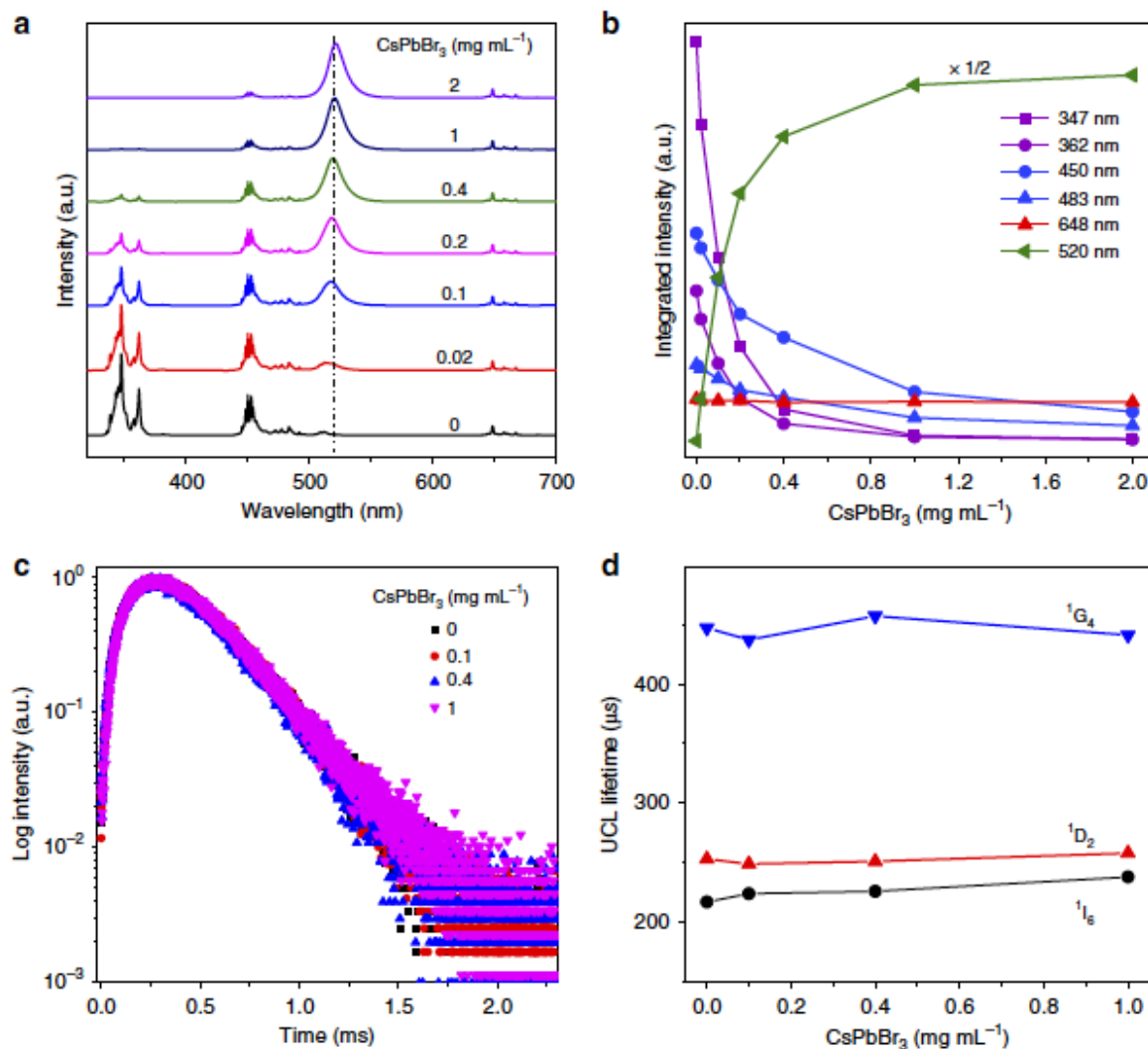


**Figure 5.** Investigation on the RET process in NP-sensitized CsPbX<sub>3</sub> perovskite NCs. (a) CsPbBr<sub>3</sub> concentration-dependent UCL spectra for LiYbF<sub>4</sub>:0.5%Tm<sup>3+</sup>@LiYF<sub>4</sub> core/shell NP (1 mg·mL<sup>-1</sup>)-sensitized CsPbBr<sub>3</sub> perovskite NCs excited at 980 nm; (b) integrated intensities for Tm<sup>3+</sup> emissions and CsPbBr<sub>3</sub> emission at 520 nm vs. the CsPbBr<sub>3</sub> concentration from (a); (c) UCL decays from <sup>1</sup>D<sub>2</sub> of Tm<sup>3+</sup> by monitoring the Tm<sup>3+</sup> emission at 362 nm in NP-sensitized CsPbBr<sub>3</sub> perovskite NCs with various concentrations excited at 980 nm; (d) UCL lifetimes of <sup>1</sup>I<sub>6</sub>, <sup>1</sup>D<sub>2</sub> and <sup>1</sup>G<sub>4</sub> of Tm<sup>3+</sup> in NP-sensitized CsPbBr<sub>3</sub> perovskite NCs vs. the CsPbBr<sub>3</sub> concentration. Reprinted with permission [74]. Copyright 2018, Nature Publishing.

Furthermore, there is a great need to develop heterostructured NCs based on inorganic perovskites. More clearly, although perovskite QDs have excellent optical properties, their biological applications have not been explored much because of their poor stability and the short penetration depth of UV light into tissues. The combination of perovskite QDs with Ln NPs has provided stable hybrid NCs, which are NIR excitable and emission tuneable. Hence, Ruan et al. [75] synthesized perovskite–Ln NP hybrid NCs composed of perovskite NCs with cubic phase and Ln NPs with hexagonal phase. The heterostructured CsPbBr<sub>3</sub>–NaYF<sub>4</sub>:Yb,Tm NCs were synthesized in one pot and consisted of cubic-phase CsPbBr<sub>3</sub> QDs embedded in hexagonal-phase NaYF<sub>4</sub>:Yb,Tm NPs, which thus formed a

watermelon structure with multiple seeds, and a cubic-phase  $\text{NaYF}_4:\text{Yb},\text{Tm}$  NP was used as an intermediate transition phase. The hybrid NCs emitted the characteristic green fluorescence of  $\text{CsPbBr}_3$  QDs under UV light and UV-blue fluorescence under NIR light excitation of  $\text{NaYF}_4:\text{Yb},\text{Tm}$  NPs, thus revealing the co-existence of both  $\text{CsPbBr}_3$  and  $\text{NaYF}_4:\text{Yb},\text{Tm}$  in the same structure. Moreover, a green fluorescence was obtained upon NIR excitation when the  $\text{NaYF}_4:\text{Yb},\text{Tm}$  phase absorbed NIR light and transferred the energy to the  $\text{CsPbBr}_3$  phase. This work opens a new way for synthesizing heterostructured NCs that could be applied to many other materials.

Recently, Shao et al. [76] reported the sensitized emission of  $\text{CsPbI}_3$  perovskite NCs after NIR excitation of  $\text{CaF}_2:\text{Yb}^{3+}/\text{Ho}^{3+}$  as hierarchical nanospheres (HNSs) in  $\text{CsPbI}_3$  and  $\text{CaF}_2:\text{Yb}^{3+}/\text{Ho}^{3+}$  nanocomposite structures. By introducing an appropriate proportion of Br ions into the perovskite, the luminescence was tuned between 695 nm and 655 nm, as depicted in Figure 6. Moreover, the lifetime of  $\text{CsPbI}_3$  emissions was lengthened to several milliseconds due to energy transfer from long-lived  $\text{Ho}^{3+}$  to  $\text{CsPbI}_3$  perovskite NCs. The stability of  $\text{CsPbI}_3$  NCs was enhanced in the composites, which kept 90% of its PL after 30 days. The composites were printed on flexible substrates for dual-mode fluorescent encryption anti-counterfeiting application and possessed excellent fluorescence under the excitation of both UV and NIR light. Moreover, the  $\text{CsPbI}_3\text{-CaF}_2:\text{Yb}^{3+}/\text{Ho}^{3+}$  nanocomposites proved to be highly water-soluble, ultrastable and highly biocompatible in cell imaging applications. This work provides a new strategy for developing photon UC in perovskite NCs and a new trial for the development of multifunctional materials.

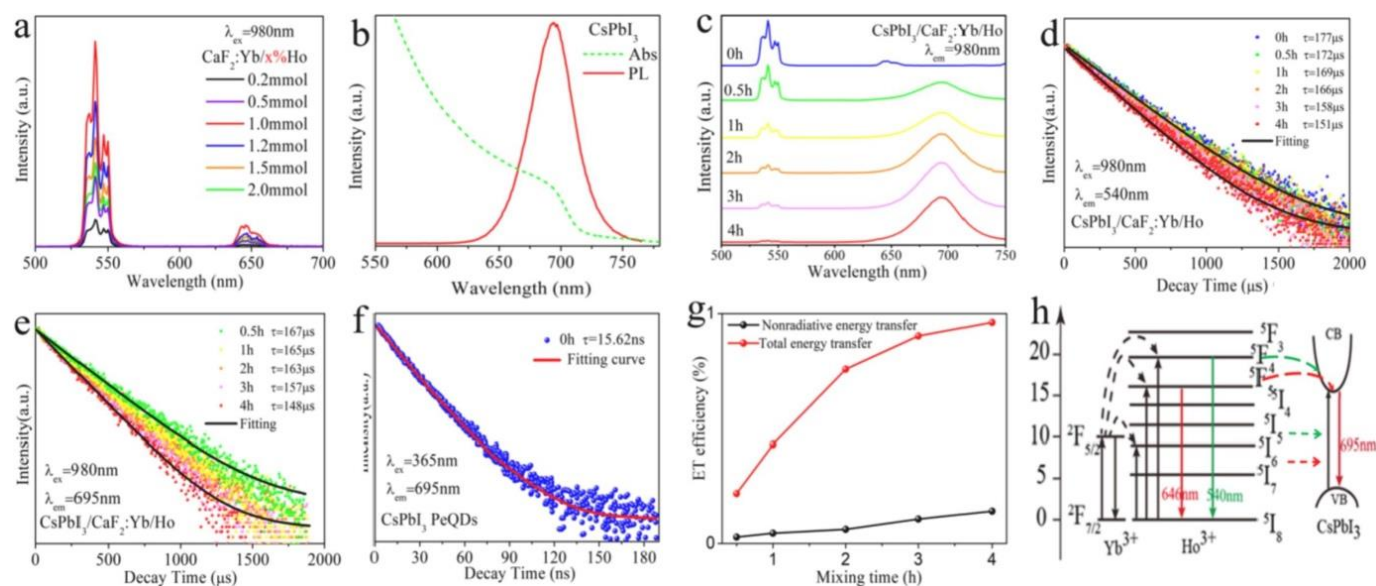


**Figure 6.** (a) UC emission spectra for  $\text{CaF}_2:\text{Yb}^{3+}$  (20%)/ $\text{Ho}^{3+}$  (x%) HNSs; (b) absorption and excitonic emission spectra for  $\text{CsPbI}_3$  perovskite NCs; (c) UC emission spectra for HNS-perovskite NCs; dynamics of emissions for  $\text{CsPbI}_3$  perovskite NCs at (d) 540 nm, (e) 695 nm and (f) 695 nm; (g) calculated energy transfer efficiency of HNS-perovskite NCs with various times obtained from (c,d); (h) mechanism of UC emission in  $\text{CsPbI}_3$  and  $\text{CaF}_2:\text{Yb}^{3+}/\text{Ho}^{3+}$  composites. Reprinted with permission [76]. Copyright 2021, Elsevier.

Although the halide perovskite nanomaterials with superior linear properties are greatly employed in optoelectronics and photonics, their strong multiphoton absorption only makes them prospective for bioimaging applications. However, the instability of perovskites in aqueous solutions limited their biological applications. Talianov et al. [77] demonstrated their fluorescence and UCL imaging in living cells using  $\text{CsPbBr}_3$  NCs with improved water resistance for at least 24 h after their coating as individual particles with various silica-based shells. The quality of  $\text{phTEOS-TMOS@CsPbBr}_3$  NCs was confirmed by HRTM and SEM, X-ray diffraction analysis, Fourier-transform infrared and

energy-dispersive X-ray spectroscopies as well as fluorescence optical microscopy. phTEOS-TMOS@CsPbBr<sub>3</sub> NCs have enhanced water stability, and consequently, they are of interest for several bioimaging applications.

In addition, it is important to note that, Estebanez et al., designed 1D-ordered nanostructures comprising Ln NPs and IHP NCs with open peapod-like shells, which were provided by a PbSO<sub>4</sub> polymer for the first time [78]. The sensitized emission of IHP was achieved by NIR excitation of nearby Ln NPs. Ln NPs with a NaYF<sub>4</sub> matrix doped with Yb and Tm or Er and with an inert shell of NaYF<sub>4</sub>, in the case of core-shell Ln NPs, and all-inorganic CsPbX<sub>3</sub> NPs were selected for these studies. Interestingly, the lead sulphate shell enhanced the luminescence of core-shell Ln NPs in the polymers by ≈20 fold, which plays an important role in the efficiency of sensitized emission of LHNPs under NIR excitation of Ln NP-IHP NC co-polymers as well as in the chemical stability of IHP NCs in contact with water. In addition, the co-polymers were prepared as colloids and deposited as solid films on a glass substrate. The lifetime of sensitized IHP emission and emission efficiency entirely depended on irradiance and sample conditions. These co-polymers are promising candidates for manufacturing the photonic devices. Table 1 summarizes the various applications of Ln-doped and undoped IHPs by means of a UC process.

**Table 1.** Lanthanide-doped inorganic halide perovskite NCs and non-doped perovskites for various applications.

S.No	Perovskites	Lanthanide Ions	Description	Application	Ref.
1	CsPbCl <sub>3</sub> NCs	Ce <sup>3+</sup> , Sm <sup>3+</sup> , Eu <sup>3+</sup> , Tb <sup>3+</sup> , Dy <sup>3+</sup> and Er <sup>3+</sup>	The introduction of lanthanide ions can considerably improve the PLQY of CsPbCl <sub>3</sub> NCs and can provide visible light emissions and even NIR emissions.	Light emitting and other photoelectronic devices	[79]
2	CsPbCl <sub>3</sub>	Bi <sup>3+</sup> /Mn <sup>2+</sup>	The co-doped perovskite exhibits tuneable emissions spanning the wide range of correlated colour temperature (CCT) from 19,000 K to 4250 K under UV excitation. This interesting spectroscopic behaviour benefits from efficient energy transfer from the perovskite NCs to intrinsic energy levels of Bi <sup>3+</sup> or Mn <sup>2+</sup> doping ions.	Lighting and displays	[80]
3	CsPbCl <sub>3</sub> NCs	Yb <sup>3+</sup> and Yb <sup>3+</sup> /Er <sup>3+</sup>	The Yb <sup>3+</sup> -doped CsPbCl <sub>3</sub> NCs emit strong NIR light at 986 nm, whereas the Yb <sup>3+</sup> /Er <sup>3+</sup> co-doped CsPbCl <sub>3</sub> NCs emit at 1533 nm. The total PLQY of the CsPbCl <sub>3</sub> NCs changes from 5.0% to 127.8% upon incorporating 2.0% Yb <sup>3+</sup> , resulting in a 25.6 enhancement factor.	Diode lasers and photo-communications	[81]
4	CsPbX <sub>3</sub> NCs	CaF <sub>2</sub> : Ln (Ln = Yb <sup>3+</sup> /Er <sup>3+</sup> , Yb <sup>3+</sup> /Ho <sup>3+</sup> and Yb <sup>3+</sup> /Tm <sup>3+</sup> )	Owing to extremely high fluorescence resonance energy transfer (FRET) efficiency (~99.7%), excitonic UCL from CsPbX <sub>3</sub> is performed under a low-power density of 980 nm diode laser irradiation.	Opto-electronics and photovoltaics	[82]
5	CsPbI <sub>3</sub>	NaYF <sub>4</sub> :Yb/Tm @NaYF <sub>4</sub>	An efficient single red band UC emission of CsPbI <sub>3</sub> perovskite quantum dots (PQDs) was observed. In addition, the emission was easily regulated from 705 to 625 nm by introducing an appropriate proportion of Br ions, which is very difficult to achieve for traditional UCNPs. Moreover, benefiting from the efficient downshifting (DS) red emission of CsPbI <sub>3</sub> PQDs, the composites displayed dual-wavelength excitation characteristics.	Dual-mode anticounterfeiting application	[83]
6	CsPbBrI <sub>2</sub>	w/o lanthanides	When photons only excite electrons in shallow trap states, some excited photons are absorbed by the shallow trap state, thus producing single-photon UCPL while the remaining photons are absorbed by the valence band, resulting in electron transfer from the valence band to the conduction band. Hence, the UC process is gradually dominated by a two-photon process as the energy of the incident photons decreases.	Optoelectronics	[84]
7	CsPbBr <sub>1-x</sub> PQDs	NaYF <sub>4</sub> Ln NPs	To improve the lattice matching between UCNPs and PQDs by replacing Y instead of Gd, the heterostructured CsPbBr <sub>3</sub> -NaGdF <sub>4</sub> :Yb,Tm NCs are obtained. They exhibit enhanced luminescence as well as stability at high temperatures, in polar solvents and under continuous UV excitation when compared with CsPbBr <sub>3</sub> -NaYF <sub>4</sub> :Yb,Tm nanocrystals and pure PQDs.	Optoelectronics	[85]
8	CsPbA <sub>3</sub> (A = Cl, Br and I)	w/o lanthanides	An efficient UCPL with a striking phonon-assisted energy gain of ~8 kBT is obtained with high-quality, all-inorganic CsPbA <sub>3</sub> perovskite NCs. In non-equilibrium conditions, the acoustic phonon UC recycles the population of optical modes and boosts the efficiency of photon UC.	Optoelectronics	[86]

Table 1. Cont.

S.No	Perovskites	Lanthanide Ions	Description	Application	Ref.
9	CsPbBr <sub>3</sub>	w/o lanthanides	Vapor-phase epitaxial CsPbBr <sub>3</sub> microplatelets are obtained with high crystallinity; self-formed high-quality microcavities; and great thermal stability, low-threshold and high-quality factor whispering-gallery mode lasing under one, two and three-photon excitation, and the lasing action is very stable under continuous pulsed laser irradiation (~3.6 Å~107 laser shots).	Lasing	[87]

## 5. Other UC Luminescence Materials

Li et al. [88] designed superstructures comprising a metal-organic framework as the core and Nd<sup>3+</sup>-sensitized Ln NPs as satellites using an electrostatic self-assembly strategy. This double photosensitizer superstructure has a three-mode imaging function, including magnetic resonance, UCL and fluorescence, as well as an excellent anti-tumour effect under NIR excitation (at 808 nm) according to in vitro and in vivo experiments. Thus, the red blood cells did not deteriorate in the presence of the superstructure. Moreover, exposure of BALB/c mice to a 808 nm laser for 5 min demonstrated a lower temperature of the irradiated area, at about 42 °C, which did not result in damage to the mice. By contrast, the temperature of the irradiated area was raised to above 50 °C when using a laser excitation at 980 nm, and consequently, the mice skin was severely burned. Then, it can be proposed that the laser excitation at 808 nm is more adequate for biological applications since it produces a much weaker tissue thermal effect.

At the same time, Sun et al. [89] synthesized Ln<sup>3+</sup>-doped nanocomposites, specifically NaYF<sub>4</sub>:Yb<sup>3+</sup>,Er<sup>3+</sup>@NaYF<sub>4</sub>-Ce6@mSiO<sub>2</sub>-CuS nanohybrids for the applications of sensing and therapy, which provided temperature feedback in the phototherapy treatment (PTT) and were involved in photodynamic therapy treatment (PDT). NaYF<sub>4</sub>:Yb<sup>3+</sup>,Er<sup>3+</sup>@NaYF<sub>4</sub> NPs were coated with mesoporous SiO<sub>2</sub> combined with a Chlorin e6 (Ce6) photosensitizer, which can be excited by the red emission of Er<sup>3+</sup> to lead to NaYF<sub>4</sub>:Yb<sup>3+</sup>,Er<sup>3+</sup>@NaYF<sub>4</sub>-Ce6@mSiO<sub>2</sub>. Then, the citrate-capped CuS (Cit-CuS) NPs as a photothermal conversion agent were attached to the composite surface. The temperature of the PTT site was monitored by recording the I<sub>525</sub>/I<sub>545</sub> ratio of green emissions, as depicted in Figure 7. Based on the guidance obtained from spectral experiments, the dual-modal tumour therapy and real-time temperature monitoring were investigated both in vitro and in vivo, obtaining reasonable results.

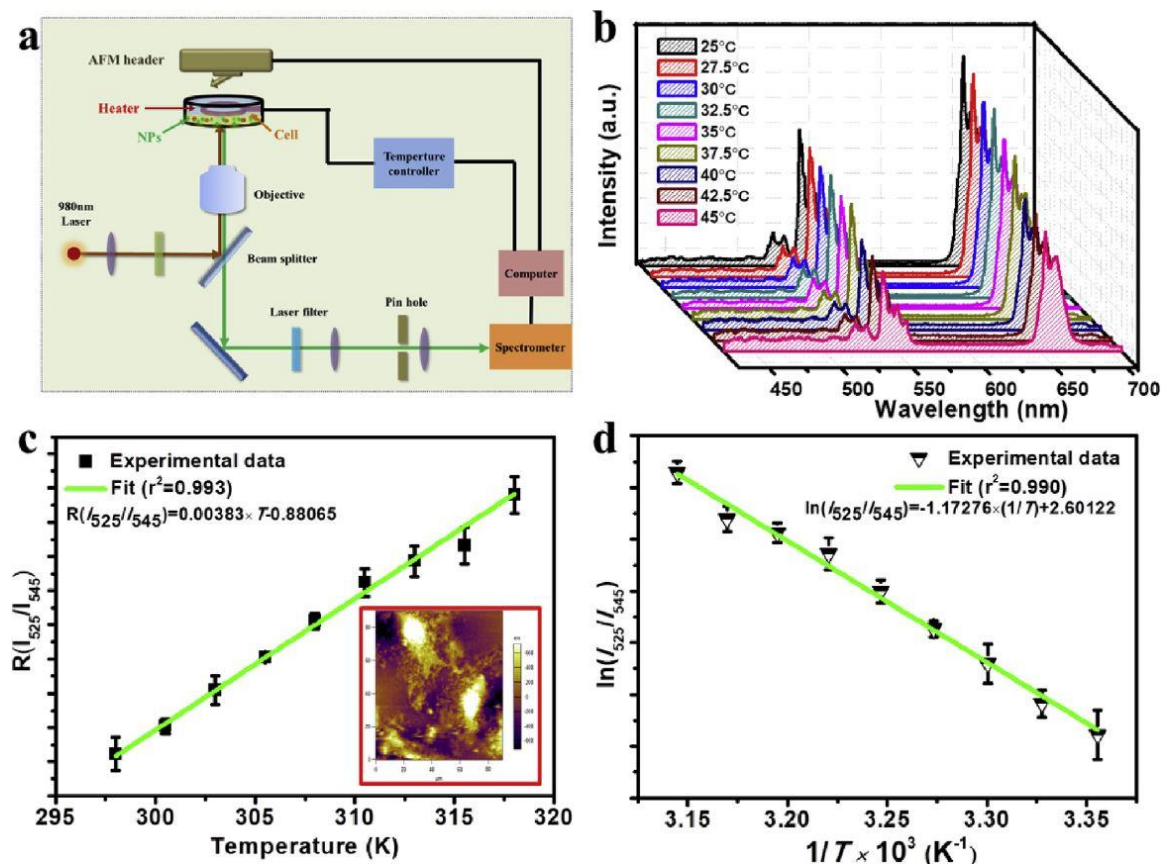


**Figure 7.** (a) Schematic diagram for the detection of temperature and emission spectrum of Ln NP-Ce6@mSiO<sub>2</sub>-CuS incubated with cells in physiological range; (b) UC emission spectra for Ln NP-Ce6@mSiO<sub>2</sub>-CuS incubated with cells at various temperatures by external heating; (c) finite impulse response (FIR) of green UC emissions for  ${}^2H_{11/2}/{}^4S_{3/2} \rightarrow {}^4I_{15/2}$  transitions based on the temperature of Ln NP-Ce6@mSiO<sub>2</sub>-CuS incubated with cells (inset: AFM image of cell after spectral detection); (d) a plot of  $\ln(I_{525}/I_{545})$  versus  $1/T$  to calibrate the thermometric scale for Ln NP-Ce6@mSiO<sub>2</sub>-CuS incubated with cells. Reprinted with permission [89]. Copyright 2019, Elsevier.

## 6. Conclusions and Perspective

In this review article, the UC emission properties of Ln-doped inorganic perovskite NPs as UC materials have been discussed. We summarized the advances in the development of these materials among others UC nanomaterials relevant for biological applications. The major challenge for transforming UC nanotechnology into real-world applications is to enhance both the brightness and emission efficiency of Ln-doped NPs.

It is important to note that the unique optical properties of Ln-doped NPs have attracted enormous scientific and technological interests. Intentional doping with higher concentration of Ln ions into different sections across a single Ln-doped NP has been explored to enhance the desirable optical properties as well as to introduce multifunctionality. Thus far, only spherical core@shell nanostructures have been reported to modulate the energy transfer, and hence, further investigations on heterogeneous one-dimensional structures, including rods, plates and dumbbells, are still needed. Importantly, controlled growth towards atomic precision is highly recommended for a clear understanding of these sophisticated energy transfer processes and the tuning of UC emissions. More clearly, the arrangement of dopants with higher concentrations into a host matrix along one direction could confine a direction of energy transfer and, consequently, may create new properties and enable novel applications.

The unique optical properties of highly doped LnIHPs have a great impact in the biological and biomedical fields. It is noteworthy that small-sized and bright Ln-doped

NPs are needed to those applications, but owing to brightness issues, most of the currently developed Ln-doped NPs are relatively large (ranging between 20 and 50 nm). The synthesis of highly doped sub-10 nm level Ln-doped NPs with desirable emissions comparable with that of quantum dots and organic dyes is an extraordinarily challenging issue. Recently, the fine-tuning of Ln-doped NP with sizes below 10 nm has been achieved via homogeneous doping at high-doping concentrations. Nevertheless, the fabrication of sub-10 nm level Ln-doped NPs with heterogeneously doped core@shell nanostructures is challenging.

Despite the abovementioned advantages of Ln-doped NPs, their biological applications are limited due to their low water dispersibility. In this regard, modification of the NP surface is essential for improving their hydrophilicity and biocompatibility. There are mainly two types of modifiers: (i) organic surfactants, including cetyl-trimethyl ammonium bromide and ethylene diamine tetraacetic acid, which are mostly used as ligands to control both particle growth and stabilization against aggregation, and (ii) bifunctional polymers, such as polyvinylpyrrolidone, chitosanpolyethylenimine, polyacrylic acid sodium salt and polyethylene glycol, which are often used as chelating and stabilizing agents to render Ln-doped NPs hydrophilic and to provide functional groups for bio-conjugations.

The surface molecules not only play a crucial role in the controlled synthesis of nanomaterials but also significantly alter the luminescence properties of nanomaterials. Therefore, the recent developments in dye-sensitized Ln-doped NPs and surface phonon-enhanced Ln-doped NPs in the thermal field have become a hot topic. Usually, Ln-doped NCs exhibit a narrow band and low absorption coefficient. Interestingly, organic dyes have more than 10 times broader absorption spectra and  $10^3$ – $10^4$ -fold higher absorption cross sections than that of  $\text{Yb}^{3+}$  sensitizer ions in Ln NPs. Therefore, despite photostability issues, the dye-sensitized UC system may enhance the UC performance. The phonons at the surface of a highly  $\text{Yb}^{3+}$ -doped UC system can control thermal quenching and significantly enhance the UC brightness, particularly in sub-10 nm level NPs. Moreover, the surface plasmons on Ln-doped NPs produce greatly enhanced UC emissions, especially red emission due to the local field enhancement effect. However, further studies based on biological applications are still needed.

Furthermore, the hierarchical structures mostly possessed superior optical properties when compared with traditional NPs; specifically, core-shell composites of hydrophobic Ln-doped NPs encapsulated within a  $\text{SiO}_2$  layer have recently received extensive scientific and technological interest. The surface silica prevented NPs from flocculation and provides room for decoration with functional groups such as thiol, amino and carboxyl groups, which allowed for greater control in conjugation protocols even though precise control of both the thickness and uniformity of  $\text{SiO}_2$  layers is rather difficult and, hence, most Ln-doped NPs may be packed together in a single layer of  $\text{SiO}_2$ , which will result in aggregation. In addition, the stability of organic capping on Ln-doped NPs is crucial for efficient luminescence in aqueous solutions. Interestingly, polysulfonate (PSS) capping on a Ln-doped NP surface has been shown to be useful for preventing NP disintegration in water and provided superior stability in a highly acidic medium. For comparison, the bare Ln NPs progressively disintegrated into their compositional ions and thus caused undesirable interference in chemical or biological environments. Additionally, the PSS capping layer can be further functionalized to lead new functional Ln-doped nanohybrids. The heterostructured NCs of perovskite with Ln NPs exhibited enhanced water stability, and consequently, they are of interest for several bioimaging applications. Interestingly, Ln-doped NPs with thin PSS coating and their functionalization with DNA have recently been reported. Both Ln-doped NPs and DNA preserved their full functionality, as demonstrated by Förster resonance energy transfer hybridization assays with Cy3-conjugated complementary DNA. Ratiometric FRET from Ln-doped NP to Cy3 demonstrated that these nanohybrids are able to quantify miR20a in the  $0.01$ – $10 \times 10^{-9}$  M concentration range with a detection limit of  $30 \times 10^{-12}$  M (4.5 fmol of miR20a) [90].

While great progress has been made in the biomedical field based on Ln-doped NPs for the last few years, there remain issues that hinder the potential applications of Ln

doped NPs as therapeutic and bioimaging agents. Specifically, nanotoxicology and safety assessments are the most essential studies for clinical applications. In vitro and in vivo toxicity assessments can be used to prove that Ln-doped NPs exhibit no obvious toxicity, but the effects of Ln-doped NPs on small animals used for longer duration as well as the interaction between Ln-doped NPs and the immune system are still unknown; moreover, the interaction between Ln-doped NPs and proteins in blood is still unclear. Therefore, much more systematic investigations are still needed. For the toxicity problem, lead-free perovskite could be a promising candidate as a future research direction.

**Author Contributions:** Conceptualization, G.M.A., S.K.K., R.E.G. and J.P.-P.; methodology, G.M.A. and S.K.K.; validation, J.P.-P.; investigation, G.M.A. and S.K.K.; resources, G.M.A. and S.K.K.; writing—original draft preparation, G.M.A.; writing—review and editing, G.M.A. and S.K.K.; supervision, R.E.G. and J.P.-P.; project administration, J.P.-P.; funding acquisition, J.P.-P. All authors have read and agreed to the published version of the manuscript.

**Funding:** We thank the Spanish Ministry of Science and Innovation (MICINN) (PID2020-115710GB-I00), Agencia Estatal de Investigación-AEI, (MICIU Unit of Excellence “Maria de Maeztu” CEX2019-000919-M) and Generalitat Valenciana (PROMETEO/2019/80, PROMETEO/2020/077 and IDIFEDER/2018/064) for all partially co-financing this work with FEDER funds.

**Institutional Review Board Statement:** Not applicable.

**Informed Consent Statement:** Not applicable.

**Data Availability Statement:** Not applicable.

**Conflicts of Interest:** The authors declare no conflict of interest.

## References

1. Zhang, F.; Zhong, H.; Chen, C.; Wu, X.-G.; Hu, X.; Huang, H.; Han, J.; Zou, B.; Dong, Y. Brightly Luminescent and Color-Tunable Colloidal  $\text{CH}_3\text{NH}_3\text{PbX}_3$  ( $X = \text{Br}, \text{I}, \text{Cl}$ ) Quantum Dots: Potential Alternatives for Display Technology. *ACS Nano* **2015**, *9*, 4533–4542. [[CrossRef](#)] [[PubMed](#)]
2. Huang, H.; Bodnarchuk, M.I.; Kershaw, S.V.; Kovalenko, M.V.; Rogach, A.L. Lead Halide Perovskite Nanocrystals in the Research Spotlight: Stability and Defect Tolerance. *ACS Energy Lett.* **2017**, *2*, 2071–2083. [[CrossRef](#)] [[PubMed](#)]
3. Green, M.A.; Ho-Baillie, A.; Snaith, H.J. The emergence of perovskite solar cells. *Nat. Photonics* **2014**, *8*, 506–514. [[CrossRef](#)]
4. Yakunin, S.; Protesescu, L.; Krieg, F.; Bodnarchuk, M.I.; Nedelcu, G.; Humer, M.; De Luca, G.; Fiebig, M.; Heiss, W.; Kovalenko, M.V. Low-threshold amplified spontaneous emission and lasing from colloidal nanocrystals of caesium lead halide perovskites. *Nat. Commun.* **2015**, *6*, 8056. [[CrossRef](#)]
5. Stoumpos, C.C.; Kanatzidis, M.G. The Renaissance of Halide Perovskites and Their Evolution as Emerging Semiconductors. *Acc. Chem. Res.* **2015**, *48*, 2791–2802. [[CrossRef](#)]
6. Nedelcu, G.; Protesescu, L.; Yakunin, S.; Bodnarchuk, M.I.; Grotevent, M.J.; Kovalenko, M.V. Fast Anion-Exchange in Highly Luminescent Nanocrystals of Cesium Lead Halide Perovskites ( $\text{CsPbX}_3$ ,  $X = \text{Cl}, \text{Br}, \text{I}$ ). *Nano Lett.* **2015**, *15*, 5635–5640. [[CrossRef](#)]
7. Dey, A.; Ye, J.; De, A.; Debroye, E.; Ha, S.K.; Bladt, E.; Kshirsagar, A.S.; Wang, Z.; Yin, J.; Wang, Y.; et al. State of the Art and Prospects for Halide Perovskite Nanocrystals. *ACS Nano* **2021**, *15*, 10775–10981. [[CrossRef](#)]
8. Ma, J.; McLeod, J.A.; Chang, L.-Y.; Pao, C.-W.; Lin, B.-H.; Li, X.-Y.; Wang, Z.; Chen, J.; Sham, T.-K.; Liu, L. Increasing photoluminescence yield of  $\text{CsPbCl}_3$  nanocrystals by heterovalent doping with  $\text{Pr}^{3+}$ . *Mater. Res. Bull.* **2020**, *129*, 110907. [[CrossRef](#)]
9. Yuan, L.; Zhou, L.; Xiang, W.; Liang, X. Enhanced stability of red-emitting  $\text{CsPbI}_3\text{:Yb}^{3+}$  nanocrystal glasses: A potential luminescent material. *J. Non-Cryst. Solids* **2020**, *545*, 120232. [[CrossRef](#)]
10. Zhao, Y.; Shen, C.; Ding, L.; Liu, J.; Xiang, W.; Liang, X. Novel B-site  $\text{Cd}^{2+}$  doped  $\text{CsPbBr}_3$  quantum dot glass toward strong fluorescence and high stability for wLED. *Opt. Mater.* **2020**, *107*, 110046. [[CrossRef](#)]
11. Fu, P.; Hu, S.; Tang, J.; Xiao, Z. Material exploration via designing spatial arrangement of octahedral units: A case study of lead halide perovskites. *Front. Optoelectron.* **2021**, *14*, 252–259. [[CrossRef](#)]
12. Zheng, W.; Huang, P.; Tu, D.; Ma, E.; Zhu, H.; Chen, X. Lanthanide-doped upconversion nano-bioprobes: Electronic structures, optical properties, and biodetection. *Chem. Soc. Rev.* **2015**, *44*, 1379–1415. [[CrossRef](#)]
13. Auzel, F. Upconversion and Anti-Stokes Processes with f and d Ions in Solids. *Chem. Rev.* **2004**, *104*, 139–174. [[CrossRef](#)]
14. Chen, G.; Qiu, H.; Prasad, P.N.; Chen, X. Upconversion Nanoparticles: Design, Nanochemistry, and Applications in Theranostics. *Chem. Rev.* **2014**, *114*, 5161–5214. [[CrossRef](#)]
15. Chen, W. Nanoparticle Fluorescence Based Technology for Biological Applications. *J. Nanosci. Nanotechnol.* **2008**, *8*, 1019–1051. [[CrossRef](#)]
16. Li, H.; Wang, X.; Huang, D.; Chen, G. Recent advances of lanthanide-doped upconversion nanoparticles for biological applications. *Nanotechnology* **2019**, *31*, 072001. [[CrossRef](#)]

17. Jalani, G.; Naccache, R.; Rosenzweig, D.H.; Haglund, L.; Vetrone, F.; Cerruti, M. Photocleavable Hydrogel-Coated Upconverting Nanoparticles: A Multifunctional Theranostic Platform for NIR Imaging and On-Demand Macromolecular Delivery. *J. Am. Chem. Soc.* **2016**, *138*, 1078–1083. [[CrossRef](#)]
18. Jayakumar, M.K.G.; Idris, N.M.; Zhang, Y. Remote activation of biomolecules in deep tissues using near-infrared-to-UV upconversion nanotransducers. *Proc. Natl. Acad. Sci. USA* **2012**, *109*, 8483–8488. [[CrossRef](#)]
19. Li, H.; Liu, X.; Ying, Q.; Wang, C.; Jia, W.; Xing, X.; Yin, L.; Lu, Z.; Zhang, K.; Pan, Y.; et al. Self-Assembly of Perovskite CsPbBr<sub>3</sub> Quantum Dots Driven by a Photo-Induced Alkynyl Homocoupling Reaction. *Angew. Chem. Int. Ed.* **2020**, *59*, 17207–17213. [[CrossRef](#)]
20. Zhang, Y.; Lu, D.; Gao, M.; Lai, M.; Lin, J.; Lei, T.; Lin, Z.; Quan, L.N.; Yang, P. Quantitative imaging of anion exchange kinetics in halide perovskites. *Proc. Natl. Acad. Sci. USA* **2019**, *116*, 12648–12653. [[CrossRef](#)]
21. Zhang, Q.; Yin, Y. All-Inorganic Metal Halide Perovskite Nanocrystals: Opportunities and Challenges. *ACS Cent. Sci.* **2018**, *4*, 668–679. [[CrossRef](#)] [[PubMed](#)]
22. Pramanik, A.; Patibandla, S.; Gao, Y.; Gates, K.; Ray, P.C. Water Triggered Synthesis of Highly Stable and Biocompatible 1D Nanowire, 2D Nanoplatelet, and 3D Nanocube CsPbBr<sub>3</sub> Perovskites for Multicolor Two-Photon Cell Imaging. *JACS Au* **2021**, *1*, 53–65. [[CrossRef](#)] [[PubMed](#)]
23. Liu, Y.; Pan, G.; Wang, R.; Shao, H.; Wang, H.; Xu, W.; Cui, H.; Song, H. Considerably enhanced exciton emission of CsPbCl<sub>3</sub> perovskite quantum dots by the introduction of potassium and lanthanide ions. *Nanoscale* **2018**, *10*, 14067–14072. [[CrossRef](#)] [[PubMed](#)]
24. Zhao, Z.; Xu, W.; Pan, G.; Liu, Y.; Yang, M.; Hua, S.; Chen, X.; Peng, H.; Song, H. Enhancing the exciton emission of CsPbCl<sub>3</sub> perovskite quantum dots by incorporation of Rb<sup>+</sup> ions. *Mater. Res. Bull.* **2019**, *112*, 142–146. [[CrossRef](#)]
25. Shin, S.G.; Hur, J.; Choi, H.W. A Study on the Characteristics of Perovskite/ZnO-Based Ultraviolet Sensors. *J. Nanosci. Nanotechnol.* **2021**, *21*, 4336–4340. [[CrossRef](#)] [[PubMed](#)]
26. Lin, J.; Yang, C.; Huang, P.; Wang, S.; Liu, M.; Jiang, N.; Chen, D. Photoluminescence tuning from glass-stabilized CsPbX<sub>3</sub> (X = Cl, Br, I) perovskite nanocrystals triggered by upconverting Tm: KYb<sub>2</sub>F<sub>7</sub> nanoparticles for high-level anti-counterfeiting. *Chem. Eng. J.* **2020**, *395*, 125214. [[CrossRef](#)]
27. Correa-Baena, J.-P.; Abate, A.; Saliba, M.; Tress, W.; Jesper Jacobsson, T.; Grätzel, M.; Hagfeldt, A. The rapid evolution of highly efficient perovskite solar cells. *Energy Environ. Sci.* **2017**, *10*, 710–727. [[CrossRef](#)]
28. Liu, P.; Han, N.; Wang, W.; Ran, R.; Zhou, W.; Shao, Z. High-Quality Ruddlesden–Popper Perovskite Film Formation for High-Performance Perovskite Solar Cells. *Adv. Mater.* **2021**, *33*, 2002582. [[CrossRef](#)]
29. Xiang, H.; Liu, P.; Wang, W.; Ran, R.; Zhou, W.; Shao, Z. Towards highly stable and efficient planar perovskite solar cells: Materials development, defect control and interfacial engineering. *Chem. Eng. J.* **2021**, *420*, 127599. [[CrossRef](#)]
30. Liu, P.; Chen, Y.; Xiang, H.; Yang, X.; Wang, W.; Ran, R.; Zhou, W.; Shao, Z. Benefitting from Synergistic Effect of Anion and Cation in Antimony Acetate for Stable CH<sub>3</sub>NH<sub>3</sub>PbI<sub>3</sub>-Based Perovskite Solar Cell with Efficiency Beyond 21%. *Small* **2021**, *17*, 2102186. [[CrossRef](#)]
31. Wang, W.; Xu, M.; Xu, X.; Zhou, W.; Shao, Z. Perovskite Oxide Based Electrodes for High-Performance Photoelectrochemical Water Splitting. *Angew. Chem. Int. Ed.* **2020**, *59*, 136–152. [[CrossRef](#)]
32. Xiao, H.; Liu, P.; Wang, W.; Ran, R.; Zhou, W.; Shao, Z. Ruddlesden–Popper Perovskite Oxides for Photocatalysis-Based Water Splitting and Wastewater Treatment. *Energy Fuels* **2020**, *34*, 9208–9221. [[CrossRef](#)]
33. Han, X.; Liu, P.; Ran, R.; Wang, W.; Zhou, W.; Shao, Z. Non-metal fluorine doping in Ruddlesden–Popper perovskite oxide enables high-efficiency photocatalytic water splitting for hydrogen production. *Mater. Today Energy* **2022**, *23*, 100896. [[CrossRef](#)]
34. Xiao, H.; Liu, P.; Wang, W.; Ran, R.; Zhou, W.; Shao, Z. Enhancing the photocatalytic activity of Ruddlesden–Popper Sr<sub>2</sub>TiO<sub>4</sub> for hydrogen evolution through synergistic silver doping and moderate reducing pretreatment. *Mater. Today Energy* **2022**, *23*, 100899. [[CrossRef](#)]
35. Yang, X.; Chen, Y.; Liu, P.; Xiang, H.; Wang, W.; Ran, R.; Zhou, W.; Shao, Z. Simultaneous Power Conversion Efficiency and Stability Enhancement of Cs<sub>2</sub>AgBiBr<sub>6</sub> Lead-Free Inorganic Perovskite Solar Cell through Adopting a Multifunctional Dye Interlayer. *Adv. Funct. Mater.* **2020**, *30*, 2001557. [[CrossRef](#)]
36. Yang, X.; Wang, W.; Ran, R.; Zhou, W.; Shao, Z. Recent Advances in Cs<sub>2</sub>AgBiBr<sub>6</sub>-Based Halide Double Perovskites as Lead-Free and Inorganic Light Absorbers for Perovskite Solar Cells. *Energy Fuels* **2020**, *34*, 10513–10528. [[CrossRef](#)]
37. Yang, X.; Xie, A.; Xiang, H.; Wang, W.; Ran, R.; Zhou, W.; Shao, Z. First investigation of additive engineering for highly efficient Cs<sub>2</sub>AgBiBr<sub>6</sub>-based lead-free inorganic perovskite solar cells. *Appl. Phys. Rev.* **2021**, *8*, 041402. [[CrossRef](#)]
38. Liu, P.; Yang, X.; Chen, Y.; Xiang, H.; Wang, W.; Ran, R.; Zhou, W.; Shao, Z. Promoting the Efficiency and Stability of CsPbIBr<sub>2</sub>-Based All-Inorganic Perovskite Solar Cells through a Functional Cu<sup>2+</sup> Doping Strategy. *ACS Appl. Mater. Interfaces* **2020**, *12*, 23984–23994. [[CrossRef](#)]
39. Liu, M.; Johnston, M.B.; Snaith, H.J. Efficient planar heterojunction perovskite solar cells by vapour deposition. *Nature* **2013**, *501*, 395–398. [[CrossRef](#)]
40. Tsai, H.; Nie, W.; Blancon, J.-C.; Stoumpos, C.C.; Asadpour, R.; Harutyunyan, B.; Neukirch, A.J.; Verduzco, R.; Crochet, J.J.; Tretiak, S.; et al. High-efficiency two-dimensional Ruddlesden–Popper perovskite solar cells. *Nature* **2016**, *536*, 312–316. [[CrossRef](#)]
41. Zhang, Q.; Ha, S.T.; Liu, X.; Sum, T.C.; Xiong, Q. Room-Temperature Near-Infrared High-Q Perovskite Whispering-Gallery Planar Nanolasers. *Nano Lett.* **2014**, *14*, 5995–6001. [[CrossRef](#)] [[PubMed](#)]

42. Zhu, H.; Fu, Y.; Meng, F.; Wu, X.; Gong, Z.; Ding, Q.; Gustafsson, M.V.; Trinh, M.T.; Jin, S.; Zhu, X.Y. Lead halide perovskite nanowire lasers with low lasing thresholds and high quality factors. *Nat. Mater.* **2015**, *14*, 636–642. [[CrossRef](#)]
43. Xing, J.; Yan, F.; Zhao, Y.; Chen, S.; Yu, H.; Zhang, Q.; Zeng, R.; Demir, H.V.; Sun, X.; Huan, A.; et al. High-Efficiency Light-Emitting Diodes of Organometal Halide Perovskite Amorphous Nanoparticles. *ACS Nano* **2016**, *10*, 6623–6630. [[CrossRef](#)] [[PubMed](#)]
44. Yuan, M.; Quan, L.N.; Comin, R.; Walters, G.; Sabatini, R.; Voznyy, O.; Hoogland, S.; Zhao, Y.; Beaugregard, E.M.; Kanjanaboos, P.; et al. Perovskite energy funnels for efficient light-emitting diodes. *Nat. Nanotechnol.* **2016**, *11*, 872–877. [[CrossRef](#)] [[PubMed](#)]
45. Gurudayal; Sabba, D.; Kumar, M.H.; Wong, L.H.; Barber, J.; Grätzel, M.; Mathews, N. Perovskite–Hematite Tandem Cells for Efficient Overall Solar Driven Water Splitting. *Nano Lett.* **2015**, *15*, 3833–3839. [[CrossRef](#)] [[PubMed](#)]
46. Luo, J.; Im, J.-H.; Mayer, M.T.; Schreier, M.; Nazeeruddin, M.K.; Park, N.-G.; Tilley, S.D.; Fan, H.J.; Grätzel, M. Water photolysis at 12.3% efficiency via perovskite photovoltaics and Earth-abundant catalysts. *Science* **2014**, *345*, 1593–1596. [[CrossRef](#)]
47. Peña, M.A.; Fierro, J.L.G. Chemical Structures and Performance of Perovskite Oxides. *Chem. Rev.* **2001**, *101*, 1981–2018. [[CrossRef](#)]
48. MØLLER, C.K. Crystal Structure and Photoconductivity of Cæsium Plumbohalides. *Nature* **1958**, *182*, 1436. [[CrossRef](#)]
49. Zhang, Q.; Su, R.; Liu, X.; Xing, J.; Sum, T.C.; Xiong, Q. High-Quality Whispering-Gallery-Mode Lasing from Cesium Lead Halide Perovskite Nanoplatelets. *Adv. Funct. Mater.* **2016**, *26*, 6238–6245. [[CrossRef](#)]
50. Protesescu, L.; Yakunin, S.; Bodnarchuk, M.I.; Krieg, F.; Caputo, R.; Hendon, C.H.; Yang, R.X.; Walsh, A.; Kovalenko, M.V. Nanocrystals of Cesium Lead Halide Perovskites (CsPbX<sub>3</sub>, X = Cl, Br, and I): Novel Optoelectronic Materials Showing Bright Emission with Wide Color Gamut. *Nano Lett.* **2015**, *15*, 3692–3696. [[CrossRef](#)]
51. Bünzli, J.-C.G.; Piguët, C. Taking advantage of luminescent lanthanide ions. *Chem. Soc. Rev.* **2005**, *34*, 1048–1077. [[CrossRef](#)]
52. Binnemans, K. Lanthanide-Based Luminescent Hybrid Materials. *Chem. Rev.* **2009**, *109*, 4283–4374. [[CrossRef](#)]
53. Eliseeva, S.V.; Bünzli, J.-C.G. Lanthanide luminescence for functional materials and bio-sciences. *Chem. Soc. Rev.* **2010**, *39*, 189–227. [[CrossRef](#)]
54. Hinklin, T.R.; Rand, S.C.; Laine, R.M. Transparent, Polycrystalline Upconverting Nanoceramics: Towards 3-D Displays. *Adv. Mater.* **2008**, *20*, 1270–1273. [[CrossRef](#)]
55. Shen, J.; Sun, L.-D.; Yan, C.-H. Luminescent rare earth nanomaterials for bioprobe applications. *Dalton Trans.* **2008**, *42*, 5687–5697. [[CrossRef](#)]
56. Cheng, L.; Wang, C.; Liu, Z. Upconversion nanoparticles and their composite nanostructures for biomedical imaging and cancer therapy. *Nanoscale* **2013**, *5*, 23–37. [[CrossRef](#)]
57. Liu, Y.; Zhou, S.; Tu, D.; Chen, Z.; Huang, M.; Zhu, H.; Ma, E.; Chen, X. Amine-Functionalized Lanthanide-Doped Zirconia Nanoparticles: Optical Spectroscopy, Time-Resolved Fluorescence Resonance Energy Transfer Biodetection, and Targeted Imaging. *J. Am. Chem. Soc.* **2012**, *134*, 15083–15090. [[CrossRef](#)]
58. Mir, W.J.; Sheikh, T.; Arfin, H.; Xia, Z.; Nag, A. Lanthanide doping in metal halide perovskite nanocrystals: Spectral shifting, quantum cutting and optoelectronic applications. *NPG Asia Mater.* **2020**, *12*, 9. [[CrossRef](#)]
59. Reinhard, C.; Valiente, R.; Güdel, H.U. Exchange-Induced Upconversion in Rb<sub>2</sub>MnCl<sub>4</sub>:Yb<sup>3+</sup>. *J. Phys. Chem. B* **2002**, *106*, 10051–10057. [[CrossRef](#)]
60. Beurer, E.; Grimm, J.; Gerner, P.; Güdel, H.U. Absorption, Light Emission, and Upconversion Properties of Tm<sup>2+</sup>-Doped CsCaI<sub>3</sub> and RbCaI<sub>3</sub>. *Inorg. Chem.* **2006**, *45*, 9901–9906. [[CrossRef](#)]
61. Gong, S.; Li, M.; Ren, Z.; Yang, X.; Li, X.; Shen, G.; Han, G. Polarization-Modified Upconversion Luminescence in Er-Doped Single-Crystal Perovskite PbTiO<sub>3</sub> Nanofibers. *J. Phys. Chem. C* **2015**, *119*, 17326–17333. [[CrossRef](#)]
62. Wu, M.; Song, E.H.; Chen, Z.T.; Ding, S.; Ye, S.; Zhou, J.J.; Xu, S.Q.; Zhang, Q.Y. Single-band red upconversion luminescence of Yb<sup>3+</sup>–Er<sup>3+</sup> via nonequivalent substitution in perovskite KMgF<sub>3</sub> nanocrystals. *J. Mater. Chem. C* **2016**, *4*, 1675–1684. [[CrossRef](#)]
63. Ge, Y.-Y.; Zhao, Y.-J.; Yuan, X.-Y.; Sun, S.-Y.; Zhao, Y.-Z.; Zhou, H.-P. Synthesis of Er<sup>3+</sup>-doped perovskite nanorods with outstanding UC PL behavior. *RSC Adv.* **2016**, *6*, 67353–67360. [[CrossRef](#)]
64. Arumugam, G.M.; Xu, C.; Karunakaran, S.K.; Shi, Z.; Zhu, C.; Wei, M.; Feifei, Q. Efficient red up-conversion emission from Er<sup>3+</sup>-Yb<sup>3+</sup> co-doped rubidium lead iodide perovskite nanowires with surface plasmons. *Appl. Phys. Lett.* **2018**, *112*, 054104. [[CrossRef](#)]
65. Liu, C.; Gao, Z.; Zeng, J.; Hou, Y.; Fang, F.; Li, Y.; Qiao, R.; Shen, L.; Lei, H.; Yang, W.; et al. Magnetic/Upconversion Fluorescent NaGdF<sub>4</sub>:Yb,Er Nanoparticle-Based Dual-Modal Molecular Probes for Imaging Tiny Tumors in Vivo. *ACS Nano* **2013**, *7*, 7227–7240. [[CrossRef](#)]
66. Brgoch, J.; Lehner, A.J.; Chabinyk, M.; Seshadri, R. Ab Initio Calculations of Band Gaps and Absolute Band Positions of Polymorphs of RbPbI<sub>3</sub> and CsPbI<sub>3</sub>: Implications for Main-Group Halide Perovskite Photovoltaics. *J. Phys. Chem. C* **2014**, *118*, 27721–27727. [[CrossRef](#)]
67. Wang, F.; Banerjee, D.; Liu, Y.; Chen, X.; Liu, X. Upconversion nanoparticles in biological labeling, imaging, and therapy. *Analyst* **2010**, *135*, 1839–1854. [[CrossRef](#)]
68. Rinkel, T.; Raj, A.N.; Dühnen, S.; Haase, M. Synthesis of 10 nm β-NaYF<sub>4</sub>:Yb,Er/NaYF<sub>4</sub> Core/Shell Upconversion Nanocrystals with 5 nm Particle Cores. *Angew. Chem. Int. Ed.* **2016**, *55*, 1164–1167. [[CrossRef](#)]
69. Yin, W.; Zhao, L.; Zhou, L.; Gu, Z.; Liu, X.; Tian, G.; Jin, S.; Yan, L.; Ren, W.; Xing, G.; et al. Enhanced Red Emission from GdF<sub>3</sub>:Yb<sup>3+</sup>,Er<sup>3+</sup> Upconversion Nanocrystals by Li<sup>+</sup> Doping and Their Application for Bioimaging. *Chem.—Eur. J.* **2012**, *18*, 9239–9245. [[CrossRef](#)]

70. Zhou, J.; Liu, Q.; Feng, W.; Sun, Y.; Li, F. Upconversion Luminescent Materials: Advances and Applications. *Chem. Rev.* **2015**, *115*, 395–465. [[CrossRef](#)]
71. Xiang, J.; Xu, L.; Gong, H.; Zhu, W.; Wang, C.; Xu, J.; Feng, L.; Cheng, L.; Peng, R.; Liu, Z. Antigen-Loaded Upconversion Nanoparticles for Dendritic Cell Stimulation, Tracking, and Vaccination in Dendritic Cell-Based Immunotherapy. *ACS Nano* **2015**, *9*, 6401–6411. [[CrossRef](#)]
72. Hesse, J.; Klier, D.T.; Sgarzi, M.; Nsubuga, A.; Bauer, C.; Grenzer, J.; Hübner, R.; Wislicenus, M.; Joshi, T.; Kumke, M.U.; et al. Rapid Synthesis of Sub-10 nm Hexagonal NaYF<sub>4</sub>-Based Upconverting Nanoparticles using Therminol® 66. *ChemistryOpen* **2018**, *7*, 159–168. [[CrossRef](#)]
73. Kostiv, U.; Engstová, H.; Krajník, B.; Šlouf, M.; Proks, V.; Podhorodecki, A.; Ježek, P.; Horák, D. Monodisperse Core-Shell NaYF<sub>4</sub>:Yb<sup>3+</sup>/Er<sup>3+</sup>@NaYF<sub>4</sub>:Nd<sup>3+</sup>-PEG-GGGRGDSGGGY-NH<sub>2</sub> Nanoparticles Excitable at 808 and 980 nm: Design, Surface Engineering, and Application in Life Sciences. *Front. Chem.* **2020**, *8*, 497. [[CrossRef](#)]
74. Zheng, W.; Huang, P.; Gong, Z.; Tu, D.; Xu, J.; Zou, Q.; Li, R.; You, W.; Bünzli, J.-C.G.; Chen, X. Near-infrared-triggered photon upconversion tuning in all-inorganic cesium lead halide perovskite quantum dots. *Nat. Commun.* **2018**, *9*, 3462. [[CrossRef](#)]
75. Ruan, L.; Zhang, Y. NIR-excitable heterostructured upconversion perovskite nanodots with improved stability. *Nat. Commun.* **2021**, *12*, 219. [[CrossRef](#)]
76. Shao, L.; Liu, D.; Lyu, J.; Zhou, D.; Ding, N.; Sun, R.; Xu, W.; Wang, N.; Xu, S.; Dong, B.; et al. Near-infrared-pumped photon upconversion in CsPbI<sub>3</sub> and CaF<sub>2</sub>:Yb<sup>3+</sup>/Ho<sup>3+</sup> nanocomposites for bio-imaging application. *Mater. Today Phys.* **2021**, *21*, 100495. [[CrossRef](#)]
77. Talianov, P.M.; Peltek, O.O.; Masharin, M.; Khubezhov, S.; Baranov, M.A.; Drabavičius, A.; Timin, A.S.; Zelenkov, L.E.; Pushkarev, A.P.; Makarov, S.V.; et al. Halide Perovskite Nanocrystals with Enhanced Water Stability for Upconversion Imaging in a Living Cell. *J. Phys. Chem. Lett.* **2021**, *12*, 8991–8998. [[CrossRef](#)]
78. Estebanez, N.; Cortés-Villena, A.; Ferrera-González, J.; González-Béjar, M.; Galian, R.E.; González-Carrero, S.; Pérez-Prieto, J. Linear Coassembly of Upconversion and Perovskite Nanoparticles: Sensitized Upconversion Emission of Perovskites by Lanthanide-Doped Nanoparticles. *Adv. Funct. Mater.* **2020**, *30*, 2003766. [[CrossRef](#)]
79. Pan, G.; Bai, X.; Yang, D.; Chen, X.; Jing, P.; Qu, S.; Zhang, L.; Zhou, D.; Zhu, J.; Xu, W.; et al. Doping Lanthanide into Perovskite Nanocrystals: Highly Improved and Expanded Optical Properties. *Nano Lett.* **2017**, *17*, 8005–8011. [[CrossRef](#)]
80. Shao, H.; Bai, X.; Cui, H.; Pan, G.; Jing, P.; Qu, S.; Zhu, J.; Zhai, Y.; Dong, B.; Song, H. White light emission in Bi<sup>3+</sup>/Mn<sup>2+</sup> ion co-doped CsPbCl<sub>3</sub> perovskite nanocrystals. *Nanoscale* **2018**, *10*, 1023–1029. [[CrossRef](#)]
81. Zhang, X.; Zhang, Y.; Zhang, X.; Yin, W.; Wang, Y.; Wang, H.; Lu, M.; Li, Z.; Gu, Z.; Yu, W.W. Yb<sup>3+</sup> and Yb<sup>3+</sup>/Er<sup>3+</sup> doping for near-infrared emission and improved stability of CsPbCl<sub>3</sub> nanocrystals. *J. Mater. Chem. C* **2018**, *6*, 10101–10105. [[CrossRef](#)] [[PubMed](#)]
82. Ma, Y.; Wei, Y.; Jiang, F.; Liu, Y.; Hong, M. Photon upconversion of all-inorganic CsPbX<sub>3</sub> quantum dots based on fluorescence resonance energy transfer in hetero-structured perovskite/upconversion nanocomposites. *J. Lumin.* **2022**, *242*, 118565. [[CrossRef](#)]
83. Zhu, Y.; Zhao, J.; Li, X.; Xu, X.; Huang, J.; Ji, X.; Yang, G.; Pan, G. Stable and Efficient Upconversion Single Red Emission from CsPbI<sub>3</sub> Perovskite Quantum Dots Triggered by Upconversion Nanoparticles. *Inorg. Chem.* **2021**, *60*, 2649–2655. [[CrossRef](#)] [[PubMed](#)]
84. Ye, S.; Zhao, M.; Yu, M.; Zhu, M.; Yan, W.; Song, J.; Qu, J. Mechanistic Investigation of Upconversion Photoluminescence in All-Inorganic Perovskite CsPbBr<sub>2</sub> Nanocrystals. *J. Phys. Chem. C* **2018**, *122*, 3152–3156. [[CrossRef](#)]
85. Ruan, L.; Zhang, Y. Upconversion Perovskite Nanocrystal Heterostructures with Enhanced Luminescence and Stability by Lattice Matching. *ACS Appl. Mater. Interfaces* **2021**, *13*, 51362–51372. [[CrossRef](#)]
86. Del Águila, A.G.; Do, T.T.H.; Xing, J.; Jee, W.J.; Khurgin, J.B.; Xiong, Q. Efficient up-conversion photoluminescence in all-inorganic lead halide perovskite nanocrystals. *Nano Res.* **2020**, *13*, 1962–1969. [[CrossRef](#)]
87. Shi, Z.; Zhang, F.; Yan, J.; Zhang, Y.; Chen, X.; Chen, S.; Wu, D.; Li, X.; Zhang, Y.; Shan, C. Robust frequency-upconversion lasing operated at 400 K from inorganic perovskites microcavity. *Nano Res.* **2022**, *15*, 492–501. [[CrossRef](#)]
88. Li, Z.; Qiao, X.; He, G.; Sun, X.; Feng, D.; Hu, L.; Xu, H.; Xu, H.-B.; Ma, S.; Tian, J. Core-satellite metal-organic framework@upconversion nanoparticle superstructures via electrostatic self-assembly for efficient photodynamic theranostics. *Nano Res.* **2020**, *13*, 3377–3386. [[CrossRef](#)]
89. Sun, X.; Sun, J.; Dong, B.; Huang, G.; Zhang, L.; Zhou, W.; Lv, J.; Zhang, X.; Liu, M.; Xu, L.; et al. Noninvasive temperature monitoring for dual-modal tumor therapy based on lanthanide-doped up-conversion nanocomposites. *Biomaterials* **2019**, *201*, 42–52. [[CrossRef](#)]
90. Francés-Soriano, L.; Estebanez, N.; Pérez-Prieto, J.; Hildebrandt, N. DNA-Coated Upconversion Nanoparticles for Sensitive Nucleic Acid FRET Biosensing. *Adv. Funct. Mater.* **2022**, 2201541. [[CrossRef](#)]